Measurement of the Deuteron Tensor Structure Function b_1 with SoLID.

A Letter of Intent to Jefferson Lab PAC-49

E. Long,[†] K. Slifer[†‡],
L. Kurbany, M. McClellan, E. Mustafa, D. Ruth
University of New Hampshire, Durham, NH 03861

Abstract

The leading twist tensor structure function b_1 of spin-1 hadrons provides a unique tool to study partonic effects, while also being sensitive to coherent nuclear properties in the simplest nuclear system. At low x, shadowing effects are expected to dominate b_1, while at larger values, b_1 provides a clean probe of exotic QCD effects, such as hidden color due to 6-quark configuration. Since the deuteron wave function is relatively well known, any novel effects are expected to be readily observable. All available models predict a small or vanishing value of b_1 at moderate x. However, the first measurement of b_1 at HERMES revealed a crossover to an anomalously large negative value in the region $0.2 < x < 0.5$, although with relatively large experimental uncertainty.

We propose an inclusive measurement of the deuteron tensor asymmetry in the region $0.05 < x < 0.7$, for $0.8 < Q^2 < 6.5$ GeV^2 using 6.6 and 8.8 GeV incident beam energies, and the Hall A SoLID detector. With 14 days production running (half of the total time at each incident energy), we can determine b_1 with sufficient precision to discriminate between conventional nuclear models, and the more exotic behavior which is hinted at by the HERMES data. The 6.6 GeV data will be taken simultaneously with a quasi-elastic measurement of A_{zz}, which is being submitted as a separate Letter of Intent. The JLab/UVa polarized ND_3 target will be used, along with the Hall A SoLID detector, and an unpolarized 100nA beam. An additional 3.0 days will be needed for overhead. We are submitting this as an LOI because we have not yet run a full simulation of the SoLID detector. Instead we have approximated rates based on the average acceptance and detector characteristics. We've assumed a tensor polarization of 25% in this proposal, which is the tensor polarization that arises in a standard P_z= 56% vector polarized ND_3 target. There is an ongoing effort at UNH and UVa to enhance P_{zz} which will likely increase the tensor polarization beyond 25%, although we make no assumptions about the success of that program in this document.

This measurement will provide access to the tensor quark polarization, and allow a test of the Close-Kumano sum rule, which vanishes in the absence of tensor polarization in the quark sea. Until now, tensor structure has been largely unexplored, so the study of these quantities holds the potential of initiating a new field of spin physics at Jefferson Lab.

[†]Spokesperson
[‡]Contact Spokesperson

Contents

1 Background and Motivation

The deuteron is the simplest nuclear system, and in many ways it is as important to understanding bound states in QCD as the hydrogen atom was to understanding bound systems in QED. Unlike it's atomic analogue, our understanding of the deuteron remains unsatisfying both experimentally and theoretically. A deeper understanding of the deuteron's tensor structure will help to clarify how the gross properties of the nucleus arise from the underlying partons. This provides novel information about nuclear structure, quark angular momentum, and the polarization of the quark sea that is not accessible in spin-1/2 targets.

In particular, a measurement of the deuteron's tensor structure function b_1 is of considerable interest since it provides a clear measure of possible exotic effects in nuclei, i.e. the extent to which the nuclear ground state deviates from being a composite of nucleons only [1]. Such a measurement is further motivated by its connection with the spin-1 angular momentum sum rule [2].

Jefferson Lab is the ideal place to investigate tensor structure in a deuteron target at intermediate and large x. We describe such a measurement in this proposal.

1.1 Tensor Structure of the Deuteron

When a spin 1 system such as the deuteron is subjected to a magnetic field along the z-axis, the Zeeman interaction gives rise to three magnetic sublevels $I_z = +1, 0, -1$ with population fractions p_+, p_-, p_0, respectively. These populations are described by both a vector polarization,

$$\begin{aligned} P_z &= \langle I_z/I \rangle \\ &= (p_+ - p_0) + (p_0 - p_+) = p_+ - p_- \end{aligned} \tag{1}$$

and a tensor polarization [3]:

$$\begin{aligned} P_{zz} &= \langle 3I_z^2 - I(I+1) \rangle / I^2 \\ &= (p_+ - p_0) - (p_0 - p_-) = 1 - 3p_0 \end{aligned} \tag{2}$$

which are subject to the overall normalization $p_+ + p_- + p_0 = 1$.

Fig. 1 graphically demonstrates the dependence of the two nucleon distribution on the spin projection. If the two nucleons are in a relative $m = 0$ state, the surface of constant density is toroidal, while if they are in the $m = \pm 1$ state, the surface has a dumbbell shape.

In the case of deuteron spins in thermal equilibrium with the solid lattice, and neglecting the small quadrupole interaction [3], the tensor polarization is related to the vector polarization via:

$$P_{zz} = 2 - \sqrt{4 - 3P_z^2} \tag{3}$$

The maximum absolute value of $P_{zz} = -2$ occurs only for vanishing populations in the $m = \pm 1$ states. If, on the other hand, only the $m = 1$ or $m = -1$ state are occupied, the vector polarization reaches its maximum value of $+1$, and $P_{zz} = +1$.

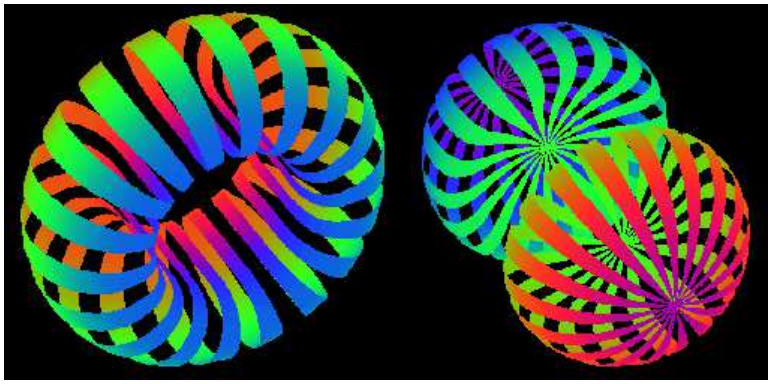

Figure 1: Nucleon densities of the deuteron in its two spin projections, $I_z = 0$ (left) and $I_z = \pm 1$ (right), respectively. *Reproduced from [4, 5].*

1.2 Deep Inelastic Scattering from Spin-1 Targets

Four independent helicity amplitudes are sufficient to describe virtual Compton scattering from a spin-1/2 target, after requiring parity and time reversal invariance. This number doubles for a spin-1 target, as the spin can be in three states (+, 0, -). This gives rise to a tensor structure which was first discussed for the deuteron for the real photon case by Pais [6], and later in the virtual photon case, by Frankfurt and Strikman [7]. Hoodbhoy, Jaffe and Manohar [8] introduced the notation which we now follow, whereby the tensor structure is described by the four functions b_1, b_2, b_3 and b_4. To summarize, the hadronic tensor can be decomposed as:

$$\begin{aligned} W_{\mu\nu} &= -F_1 g_{\mu\nu} + F_2 \frac{P_\mu P\nu}{\nu} \\ &\quad -b_1 r_{\mu\nu} + \frac{1}{6} b_2 (s_{\mu\nu} + t_{\mu\nu} + u_{\mu\nu}) \\ &\quad + \frac{1}{2} b_3 (s_{\mu\nu} - u_{\mu\nu}) + \frac{1}{2} b_4 (s_{\mu\nu} - t_{\mu\nu}) \\ &\quad + i \frac{g_1}{\nu} \epsilon_{\mu\nu\lambda\sigma} q^\lambda s^\sigma + i \frac{g_2}{\nu^2} \epsilon_{\mu\nu\lambda\sigma} q^\lambda (p \cdot q s^\sigma - s \cdot q p^\sigma) \end{aligned} \tag{4}$$

where the purely kinematic expressions $r_{\mu\nu}$, $s_{\mu\nu}$, $t_{\mu\nu}$ and $u_{\mu\nu}$ can be found in [8]. The terms are all proportional to the polarization of the target E. The spin-1 structure functions F_1, F_2, g_1 and g_2 have the same expressions and are measured the same way as for a spin-1/2 target. The spin-dependent structure functions b_1, b_2, b_3, b_4 are symmetric under $\mu \leftrightarrow \nu$ and $E \leftrightarrow E^*$ and therefore can be isolated from F_1 and g_1 by unpolarized beam scattering from a polarized spin-1 target.

We focus in this document on the leading twist structure function b_1. A Callan-Gross type relation allows access to b_2 once b_1 is determined, and b_3 and b_4 do not contribute at leading twist.

1.2.1 Interpretation in the Parton Model

In the infinite momentum frame* of the parton model, the scattering of the virtual photon from a free quark with spin up (or down), which carries a momentum fraction x of the spin-m hadron, can

*All spins and momenta are along the z-axis.

be expressed through the hadronic tensor $W_{\mu\nu}^{(m)}$:

$$W_{\mu\nu}^{(1)} = \left(-\frac{1}{2}g_{\mu\nu} + \frac{x}{\nu}P_\mu P\nu \right)\Big(q_\uparrow^1(x) + q_\downarrow^1(x)\Big) + \frac{i\epsilon_{\mu\nu\lambda\sigma}q^\lambda s^\sigma}{2\nu}\Big(q_\uparrow^1(x) - q_\downarrow^1(x)\Big),$$

for a target of spin projection equal to 1 along the z-direction, and:

$$W_{\mu\nu}^{(0)} = \left(-\frac{1}{2}g_{\mu\nu} + \frac{x}{\nu}P_\mu P\nu \right)2q_\uparrow^0(x) \tag{5}$$

for a target of spin projection equal to zero along the z-direction. The tensor structure functions b_1 and b_2 can be expressed from the comparison of $W_{\mu\nu}^{(1)} - W_{\mu\nu}^{(0)}$ with Eq. 4 as follows:

$$b_1(x) = \frac{1}{2}\Big(2q_\uparrow^0(x) - q_\uparrow^1(x) - q_\downarrow^1(x)\Big) \tag{6}$$

$$b_2(x) = 2xb_1(x) \tag{7}$$

where $q_\uparrow^m$ ($q_\downarrow^m$) represents the probability to find a quark with momentum fraction x and spin up (down) in a hadron which is in helicity state m. The tensor structure function b_1 depends only on the spin-averaged parton distributions[†]

$$q^1(x) = q_\uparrow^1(x) + q_\downarrow^1(x)$$
$$q^0(x) = q_\uparrow^0(x) + q_\downarrow^0(x) = 2q_\uparrow^0(x)$$

so it can be expressed as:

$$b_1(x) = \frac{q^0(x) - q^1(x)}{2} \tag{8}$$

Explicitly, b_1 measures the difference in partonic constituency in an $|m|$=1 target and an m=0 target. From this we see that while b_1 is defined in terms of quark distributions, it interestingly depends also on the spin state of the nucleus as a whole.

1.2.2 First Measurement of $b_1(x)$ by the HERMES Collaboration

The HERMES collaboration made the first measurement [9, 10] of b_1 in 2005. The experiment explored the low x region of $0.001 < x < 0.45$ for $0.5 < Q^2 < 5$ GeV^2. An atomic beam source was used to generate a deuterium gas target with high tensor polarization. The HERA storage ring provided 27.6 GeV positrons incident on the internal gas target.

As displayed in Fig. 2, the tensor asymmetry A_{zz} was found to be non-zero at about the two sigma level, with an apparent zero crossing around $x = 0.3$. The tensor structure function b_1 exhibits a steep rise as $x \to 0$, which is qualitatively in agreement with the predictions of coherent double-scattering models. See for example Ref. [11]. The authors of Ref. [10] interpret the rapid rise at low x in terms of the same mechanism that leads to nuclear shadowing in unpolarized scattering, i.e. double scattering of the lepton, first from the proton, then from the neutron, with sensitivity to the spatial alignment of the two nucleons.

[†]since, by parity, $q_\uparrow^m = q_\downarrow^m$

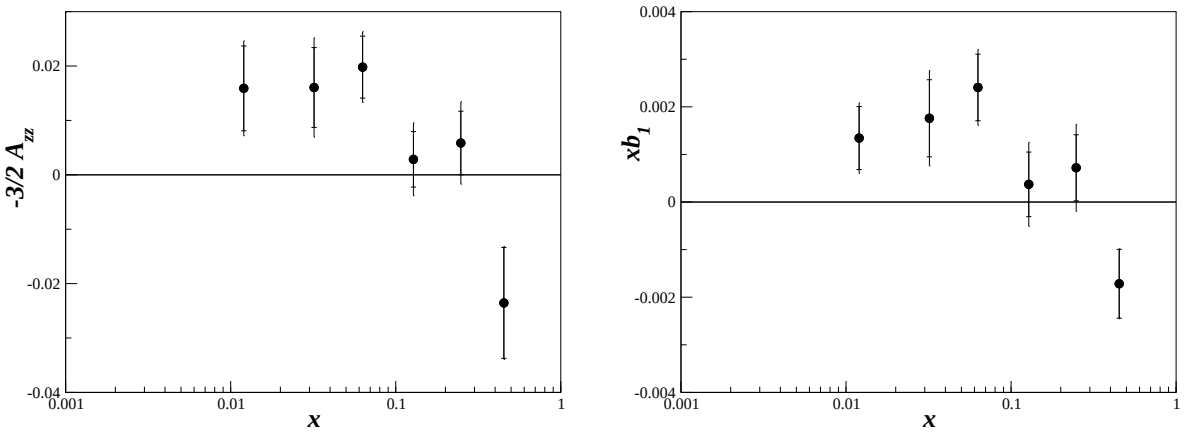

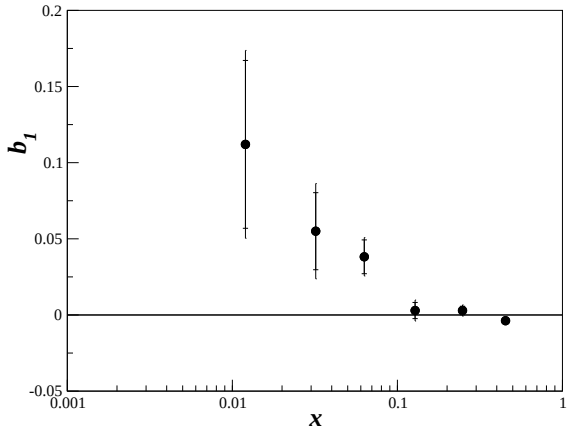

Figure 2: **Top**: HERMES [9] measurement of the inclusive tensor asymmetry $A_{zz}(x)$ and $xb_1(x)$ of the deuteron. **Bottom** : The tensor structure function $b_1(x)$ without x-weighting, which reveals a steep rise as $x \to 0$.

As is often the case with a pioneer measurement, the precision of the results leaves some room for ambiguity. Despite the surprisingly large magnitude and interesting trend of the data, all points are roughly within two sigma from zero, which calls for a higher precision measurement. Another issue is that some of the HERMES momentum transfer values are low, so that quark structure functions may not be the correct language. The Q^2 variation in each x-bin is also quite wide ($\approx$10 GeV^2 for $x \sim 0.3$), which complicates the interpretation of this data, since several models predict significant Q^2-dependence of b_1. See for example Fig. 3.

1.3 The Tensor Structure Function $b_1(x)$

The leading twist tensor structure function b_1 quantifies effects not present in the case of spin-1/2 hadrons. However, tensor effects only exist in nuclear targets, so the study of b_1 serves as a very interesting bridge between nucleon and nuclear physics. On the one hand, deep inelastic scattering (DIS), clearly probes partonic degrees of freedom, i.e. quarks, but on the other hand, b_1 depends solely on the deuteron (nuclear) spin state as seen in Eq. 7. We discuss now several predictions for the x dependence of b_1.

1.3.1 Conventional Nuclear Effects

In Ref. [8], the authors note that $b_1(x)$ is small and calculable for a weakly bound system like the deuteron, and that its measurement would provide a clear signature for exotic components in a spin one nucleus. In effect, $b_1(x)$ measures the extent to which a target nucleus deviates from a trivial bound state of protons and neutrons. The authors evaluate the value of b_1 in three conventional scenarios for the deuteron constituents and their dynamics:

I. If the deuteron is composed of two spin-1/2 non-interacting nucleons at rest, then the eight helicity amplitudes characteristic of a spin-1 target are expressed in terms of the four helicity amplitudes of each spin-1/2 nucleons, and therefore the total number of independent amplitudes is reduced from eight to four. All structure functions of the deuteron are then the simple sum of the structure functions of the two nucleons, and the tensor structure functions vanish: $b_1 = b_2 = b_3 = b_4 = 0$.

II. If instead, the deuteron is composed of two spin-1/2 nucleons moving non-relativistically in a central potential, then the target motion modifies the helicity amplitudes. Using the convolution formalism, it was found that the contribution of these moving nucleons to b_1 is small and is dominated by the lower component of the nucleon's Dirac wave function.

III. In the final scenario considered, the deuteron contains a D-state admixture. Because the proton and the neutron are moving in opposite directions, an additional term due to the $S - D$ interference appears in the convolution procedure. This extra contribution to b_1 is predicted to be even smaller than in the previous case.

All three scenarios predict a small or vanishing b_1, leading the authors to predict that $b_1 \approx 0$ for the deuteron.

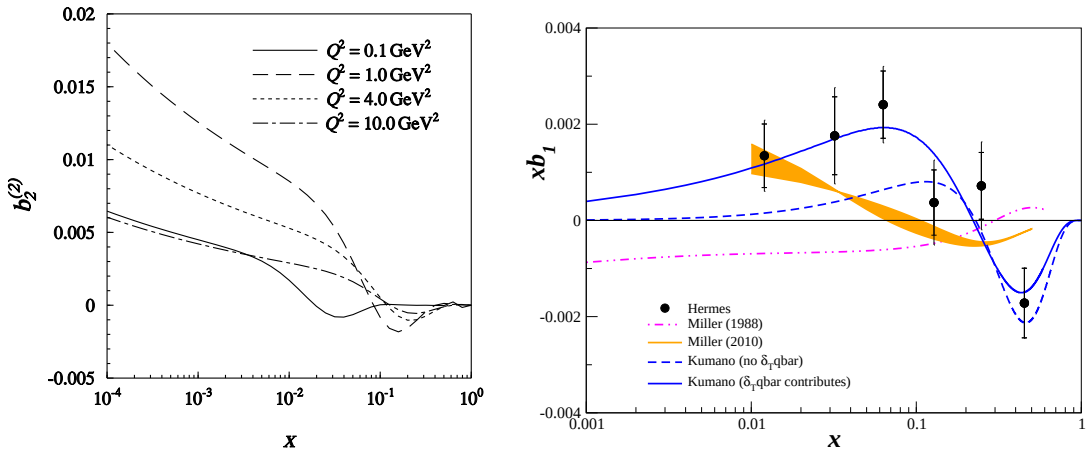

Figure 3: Theoretical predictions. **Left plot:** Double-scattering contribution to $b_2(x, Q^2)$ as a function of x [12]. Note the strong Q^2 dependence at low x. **Right plot:** HERMES results [10] compared to calculations from S. Kumano [13] and from the one-pion exchange effects of G. Miller [14, 15].

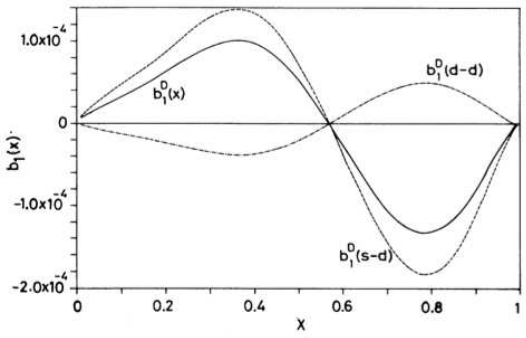

Figure 4: Prediction for $b_1^D(x)$ (solid curve) from Ref. [1], the S-D contribution to $b_1^D(x)$ (dashed curve), and the D-D contribution to $b_1^D(x)$ (dot-dashed curve). Note the vertical scale which would make the curve mostly indiscernible from zero in Fig. 3 (right). *Reproduced from Ref. [1].*

1.3.2 Nuclear Pions

In 1988, Miller also examined the tensor structure function b_1 [14]. The basic mechanism is that the virtual photon hits an exchanged pion which is responsible for the binding of the deuteron. In this early calculation, the convention used by Miller for b_1 was different from that used in the HERMES results and in Ref. [13]. A recent update to this calculation [15], which uses a consistent convention and the pion structure function from [16], is shown in Fig. 3. The spread of the curve originates from the parameter $A_s = (.9 \pm 0.3)$ which governs the strength of the sea in the pion. Miller's calculation, similar to other 'non-exotic' models, is unable to reproduce the trend of the HERMES data, and predicts very small values of $b_1(x)$ at intermediate and large x.

1.3.3 Convolution Model

Khan and Hoodbhoy [1] evaluated $b_1(x)$ in a convolution model with relativistic and binding energy corrections. They use this to evaluate the effect of nuclear Fermi motion and binding on the deuteron structure functions. They observe that for zero Fermi motion and binding $b_1^D(x) = 0$. They also predict a small enhancement of b_1 in the region of $x \sim 0.3$, as seen in Fig. 4. Note however, that the absolute scale of this predicted b_1 is $\mathcal{O}(10^{-4})$, while the HERMES data implies that the scale is more than an order of magnitude larger than this.

1.3.4 Relativistic Calculation

Umnikov [17] calculated $b_1(x)$ and $b_2(x)$ within a covariant approach, based on the relativistic convolution formalism for DIS and the Bethe-Salpeter formalism for the deuteron bound state. Fig. 5 sets the scale for $b_1(x)$ at the 10^{-3} level. Both the relativistic and non-relativistic calculations are consistent with the CK sum rule (see Sec. 1.3.8), although the nonrelativistic convolution model results in an incorrect behavior of at low x.

1.3.5 Double-Scattering Effects

Using Vector Meson Dominance (VMD), the authors of Ref. [12] isolate the double-scattering contribution to b_1. The existence time of a vector meson can be described by the coherence length:

$$\lambda = \frac{Q^2}{Mx(M_v^2 + Q^2)} \tag{9}$$

which is the length over which the vector meson propagates during the time $\Delta t = 1/\Delta E$. For significant shadowing or double scattering to occur, a minimum coherence length of ≈ 1.7 fm (the inter-nucleon separation) is required. At $x > 0.3$, the coherence length is only about the size of the nucleon, so double scattering contributions are anticipated to be negligible. However, for $x \leq 0.1$, double-scattering should be significant in b_1 behaving as $(1-x)^{2\delta}/x^{1+2\delta}$, where δ is determined from the soft pomeron intercept $\alpha_P(t=0) = 1+\delta$. The authors predicted a significant enhancement of b_1 at low x (≤ 0.01) due to the quadrupole deformation of the deuteron, which is qualitatively confirmed by the HERMES data. See Fig. 2.

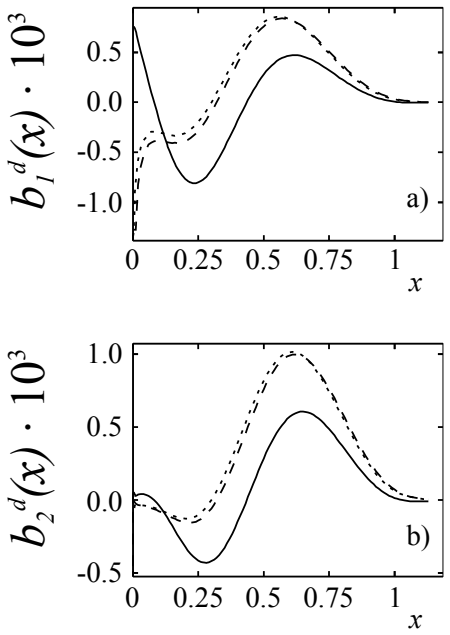

Figure 5: Relativistic convolution calculation of $b_1^D(x)$ and $b_2^D(x)$. Curves: BS - solid, Bonn - dotted, Bonn with cut -dashed. *Reproduced from Ref. [17].*

1.3.6 Virtual Nucleon Approximation

M. Sargsian [18] recently calculated the tensor asymmetry A_{zz} for deep inelastic scattering. See Figs. 6 & 7. In the approximation in which only proton-neutron component of the deuteron is taken into account and nuclear parton distributions are generated through the convolution of partonic distribution of nucleon and deuteron density matrix (see e.g. Refs. [19, 20]), the deuteron structure function b_1 is related directly to the d-partial wave of the deuteron wave function [18, 19]. As a result, this approximation predicts negligible magnitude for b_1 for $x \leq 0.6$ due to small Fermi momenta involved in the convolution integral. However, the predicted magnitude of b_1 is large at $x \geq 0.7$ where one expects substantial contribution from the d-waves due to high momentum component of the deuteron wave function involved in the convolution picture of DIS scattering off the deuteron. In this case, b_1 is very sensitive to the relativistic description of the deuteron and its measurement can be used for checking the different approximations of high momentum component of deuteron wave function.

In the calculation presented, two Virtual Nucleon and Light-Cone approximations are used to calculate the tensor polarization for DIS scattering off the deuteron. In both approximations only the proton-neutron component of the deuteron is taken into account. In the Virtual Nucleon approximation, the covariant scattering amplitude is reduced by estimating the spectator nucleon propagator at its on-energy shell in the lab frame of the deuteron. Within this approximation the baryonic sum rule is satisfied while the momentum sum rule is not. The latter is due to the fact that part of the light cone momentum of the bound virtual nucleon is lost to the unaccounted non-nucleonic degrees of freedom in the deuteron wave function. In the light cone approximation the scattering amplitude is estimated the $E + p_z$ pole of the spectator nucleon on the light cone.

In this case the wave function is defined on the light-cone reference frame and it satisfies both baryon number and momentum sum rules. For the detailed comparison of these approximations, see Ref. [20].

1.3.7 Fit to HERMES Data

Kumano [13] points out that the twist-2 structure functions b_1 and b_2 can be used to probe orbital angular momentum. He then extracts the tensor polarized quark and anti-quark distributions from a fit to the HERMES data [10]. He finds that a non-negligible tensor polarization of the sea is necessary to reproduce the trend of the data, as shown in Fig. 3. However, this conclusion has to be considered with caution due to the extended Q^2 coverage (Fig. **??**), and large uncertainty of each HERMES data point. In particular, the author calls for better measurements of b_1 at large x (> 0.2), and further investigation of the tensor structure functions in general.

1.3.8 The Close-Kumano Sum Rule

Following the formalism from the parton model in [8], Close and Kumano [21] related the tensor structure function b_1 to the electric quadrupole form factor of the spin-1 target through a sum rule[‡]:

$$\begin{aligned} \int_0^1 dx\; b_1(x) &= -\frac{5}{12M^2} \lim_{t\to 0}\; t\; F_Q(t) + \frac{1}{9}\Big(\delta Q + \delta\bar{Q}\Big)_s \\ &= \frac{1}{9}\Big(\delta Q + \delta\bar{Q}\Big)_s = 0 \end{aligned} \tag{10}$$

where $F_Q(t)$ is the electric quadrupole form factor of a spin-1 hadron at the momentum squared t. The Close Kumano (CK) sum rule is satisfied in the case of an unpolarized sea. The authors note that in nucleon-only models, the integral of b_1 is not sensitive to the tensor-polarization of the sea, and consequently the sum rule is always true, even when the deuteron is in a D-state.

The authors of Ref. [1] calculated the first moment of $b_1(x)$ in a version of the convolution model that incorporates relativistic and binding energy corrections. They found a value of -6.65$\cdot 10^{-4}$, and emphasize that deviations from this will serve as a good signature of exotic effects in the deuteron wave function. Similarly, Ref. [17] predicts $5 \cdot 10^{-4}$ and $3 \cdot 10^{-5}$ for the relativistic and nonrelativistic calculation of Eq. 10, respectively.

A truncated version of Eq. 10 was evaluated by the HERMES [9, 10] experiment and found to be:

$$\int_{0.0002}^{0.85} b_1(x)dx = 0.0105 \pm 0.0034 \pm 0.0035 \tag{11}$$

which possibly indicates a breaking of the Close-Kumano sum rule, and consequently a tensor-polarized quark sea. However, since the comparison is only at the two sigma level, more precise data is needed for a true test.

[‡]Efremov and Teryaev evidently proposed the same relation for mesons in Ref. [22].

E (GeV)	Forward Det. Physics Rates (kHz)	Forward Det. Total Rates (kHz)	Large θ Det. Physics Rates (kHz)	Large θ Det. Total Rates (kHz)	Time (days)
6.6	101	540	0.51	4.4	7
8.8	63	239	0.89	3.56	7

Table 1: Summary of the kinematics and physics rates using the SoLID detector.

$\overline{x}$	δb_1^{stat} $\times 10^{-2}$	δb_1^{sys} $\times 10^{-2}$
0.05	0.031	0.913
0.10	0.025	0.621
0.15	0.021	0.447
0.20	0.018	0.336
0.25	0.019	0.263
0.30	0.023	0.212
0.35	0.029	0.166
0.40	0.036	0.103
0.45	0.045	0.034
0.50	0.047	0.029
0.55	0.080	0.025

Table 2: Summary of the expected statistical uncertainty after combining overlapping x-bins for $E = 6.6$ GeV. Values represent the statistics weighted average of all events that satisfy our DIS cut.

2 The Proposed Experiment

We will measure the leading twist tensor structure function b_1 via the tensor asymmetry A_{zz} for $0.05 < x < 0.7$, $0.8 < Q^2 < 6.5$ GeV^2 and $W \geq 1.85$ GeV. Figs. 8, 9, 10, and 11 show the planned kinematic coverage utilizing the SoLID forward and large angle detectors with beam energies of 6.6 GeV and 8.8 GeV. The 6.6 GeV data can be taken simultaneously with a quasi-elastic measurement of A_{zz}, which is being submitted as a separate Letter of Intent.

The polarized ND_3 target is discussed in section 2.2. The magnetic field of the target will be held constant along the beamline at all times, while the target state is alternated between a polarized and unpolarized state. We are submitting this as a LOI instead of a full proposal because a full simulation of the SoLID detector has not yet been performed. Instead, an updated version of the software used in the C12-13-011 spectrometer-based proposal was used to calculate the rates. The tensor polarization and packing fraction used in the rates estimate are 25% and 0.65 , respectively. The dilution factor was calculated individually for each x bin and is approximately 0.285 on average. With an incident electron beam current of 100nA, the expected deuteron luminosity is 1.36×10^{35} / cm^2·s^1. The SoLID detector was incorporated assuming a momentum resolution of $dP/P = 2\%$, $d\theta = 0.6$ mrad, and $d\phi = 5$ mrad. The forward detector assumes an acceptance of

$\overline{x}$	δb_1^{stat} $\times 10^{-2}$	δb_1^{sys} $\times 10^{-2}$
0.05	0.717	0.716
0.1	0.555	0.554
0.15	0.427	0.426
0.2	0.330	0.329
0.25	0.256	0.255
0.3	0.197	0.196
0.35	0.152	0.151
0.4	0.117	0.115
0.45	0.087	0.084
0.5	0.061	0.056
0.55	0.041	0.032
0.6	0.033	0.017
0.65	0.032	0.012
0.7	0.044	0.008

Table 3: Summary of the expected statistical uncertainty after combining overlapping x-bins for $E = 8.8$ GeV. Values represent the statistics weighted average of all events that satisfy our DIS cut.

$8^\circ \leq \theta \leq 14.8^\circ$ and $1.0\ \mathrm{GeV}/c \leq P \leq 7.0\ \mathrm{GeV}/c$. The large angle dector assumes an acceptance of $16^\circ \leq \theta \leq 24^\circ$ and $3.5\ \mathrm{GeV}/c \leq P \leq 7.0\ \mathrm{GeV}/c$. The invariant mass W was kept to $W \geq 1.85$ GeV for all settings. The projected uncertainties for A_{zz} and b_1 are displayed in Figs. 6 and 7.

A total of 14 days of beam time is requested for production data, with an additional 3.0 days of expected overhead.

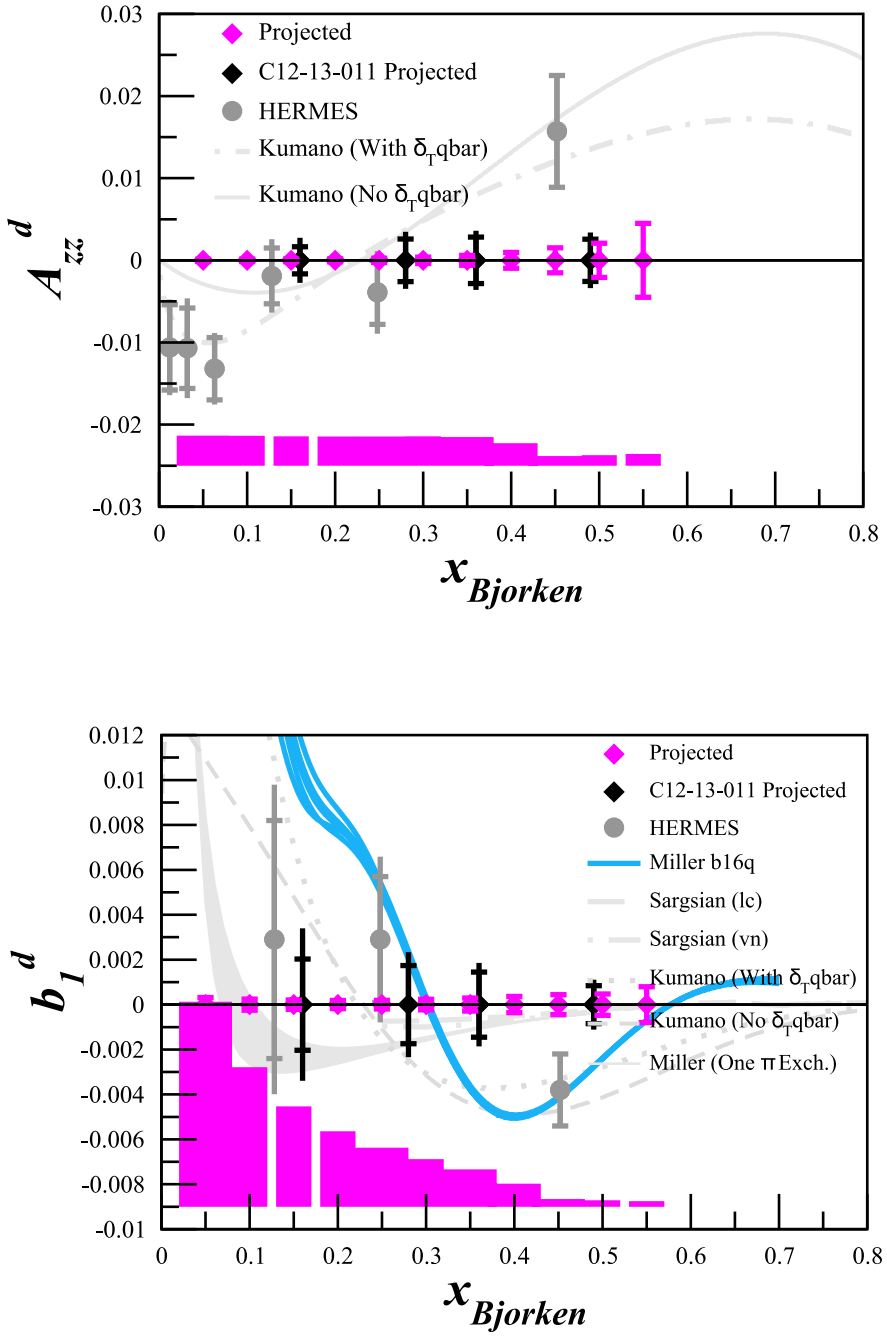

Figure 6: Projection for 7 PAC days at an incident energy of 6.6 GeV with the SoLID detector. **Top:** Projected statistical errors for the tensor asymmetry A_{zz}. **Bottom:** Projected statistical errors for the tensor structure function b_1. Data at different Q^2 are combined with an x-binning that varies slightly per point, but is approximately ± 0.05. Also shown are the HERMES data [10], and the calculations from Kumano [13], Miller [14, 15], and Sargsian [18]. The black points are the projected uncertainties for the C12-13-011 experiment in Hall C.

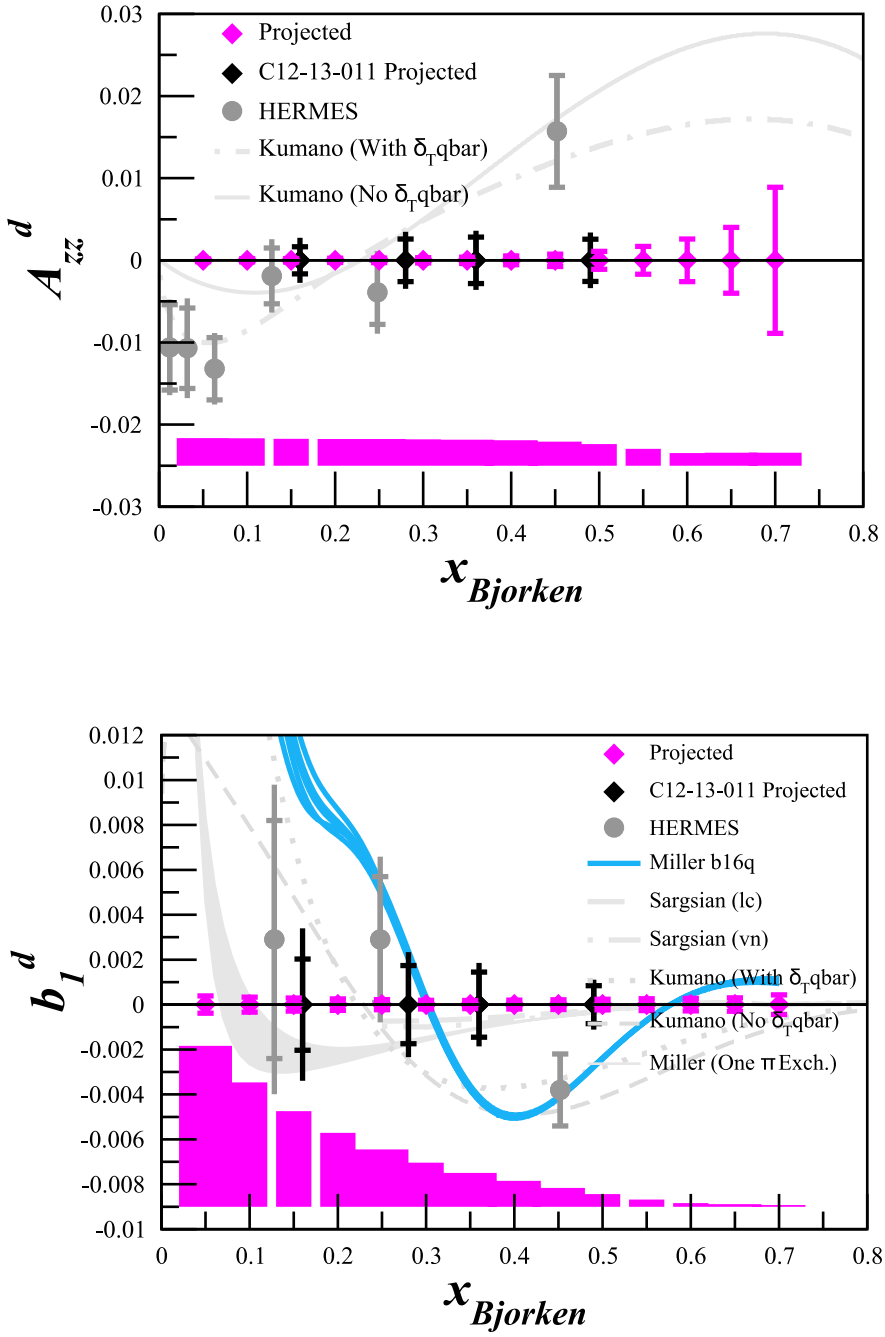

Figure 7: Projection for 7 PAC days at an incident energy of 8.8 GeV with the SoLID detector. **Top:** Projected statistical errors for the tensor asymmetry A_{zz}. **Bottom:** Projected statistical errors for the tensor structure function b_1. Data at different Q^2 are combined with an x-binning that varies slightly per point, but is approximately ± 0.05. Also shown are the HERMES data [10], and the calculations from Kumano [13], Miller [14, 15], and Sargsian [18]. The black points are the projected uncertainties for the C12-13-011 experiment in Hall C.

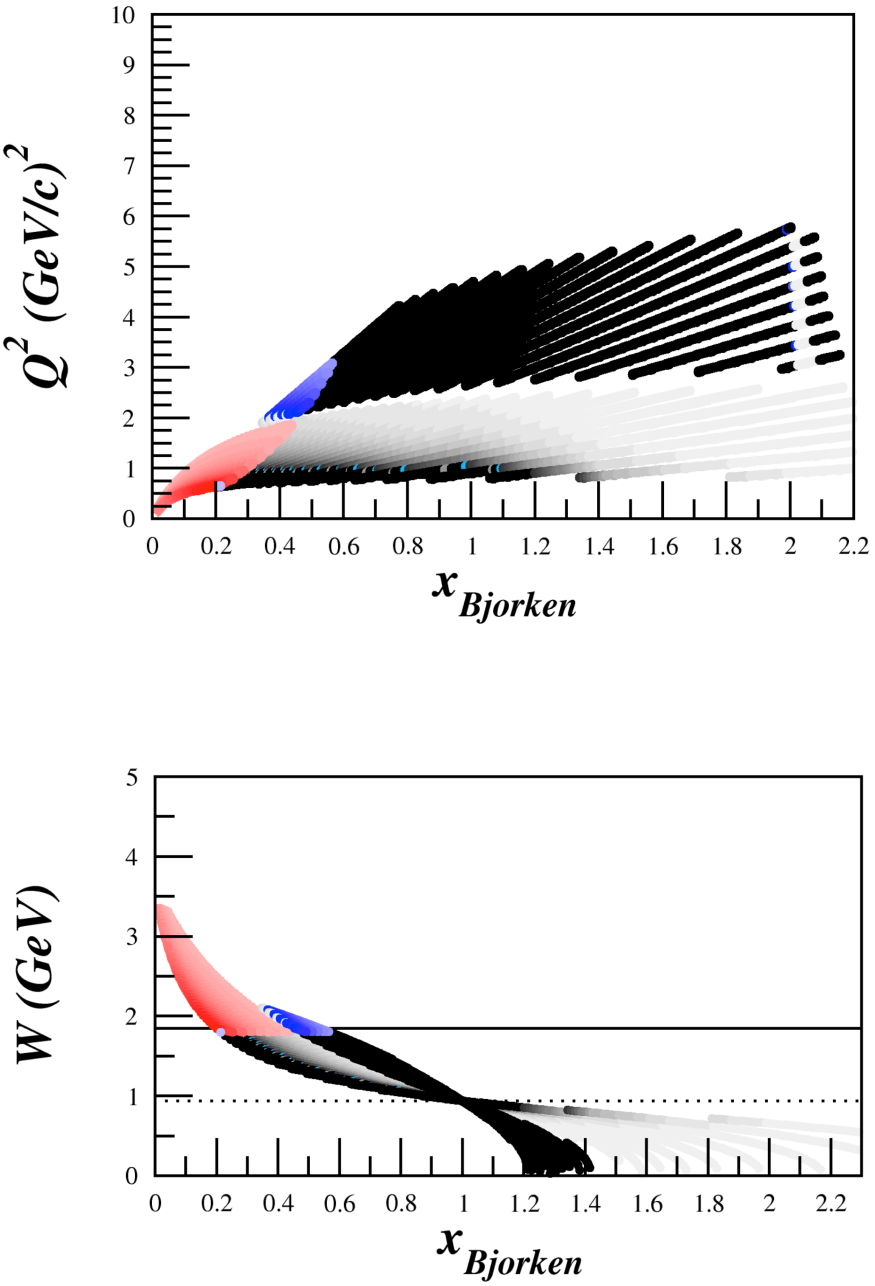

Figure 8: Kinematic coverage for incident beam energy of 6.6 GeV. The red points are for the forward detector and the blue are for the backward detector. The black/grey settings are not included in our rates estimates since they fall below $W \geq$1.85GeV.

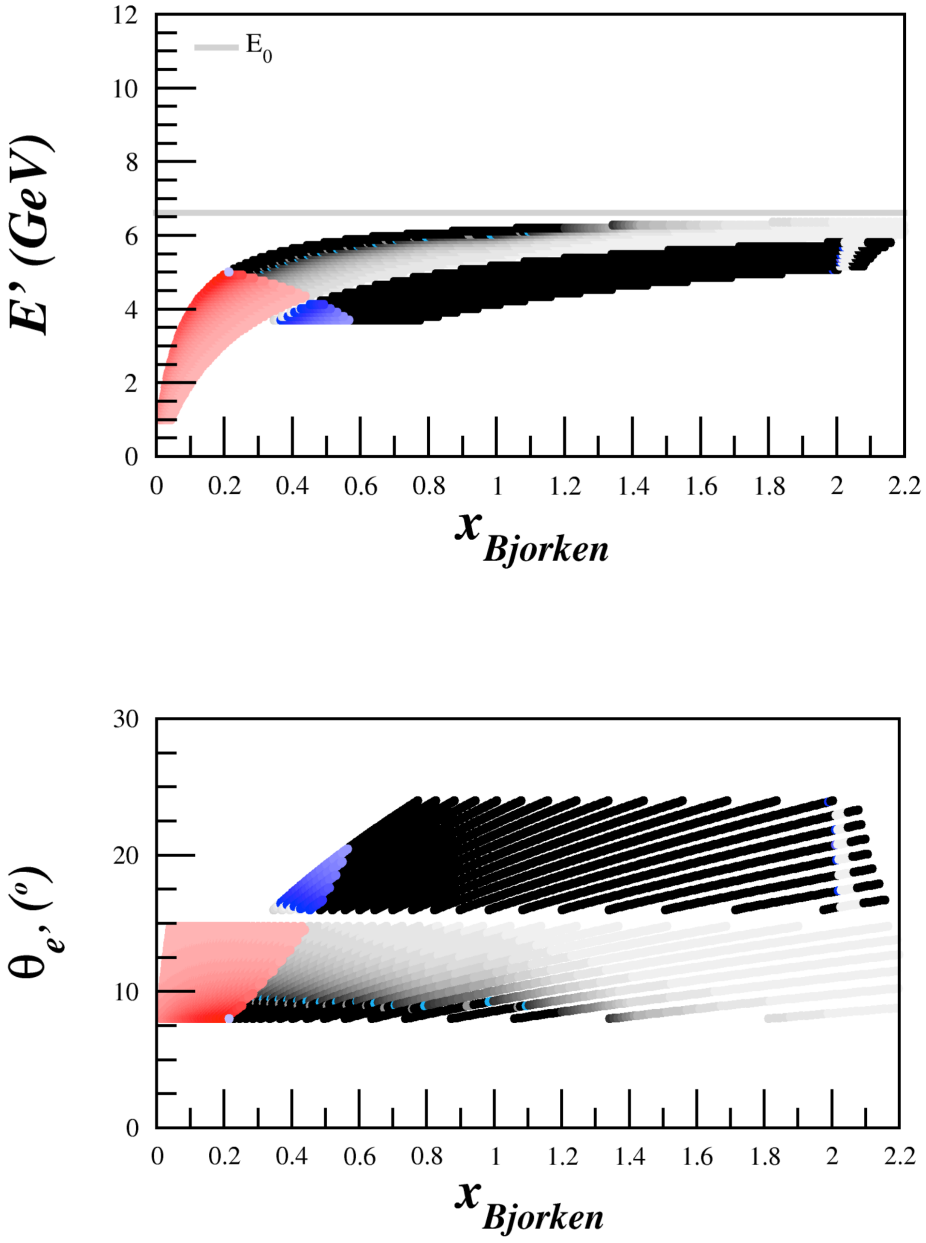

Figure 9: Kinematic coverage for incident beam energy of 6.6 GeV. The red points are for the forward detector and the blue are for the backward detector. The black/grey settings are not included in our rates estimates since they fall below $W \geq$1.85GeV.

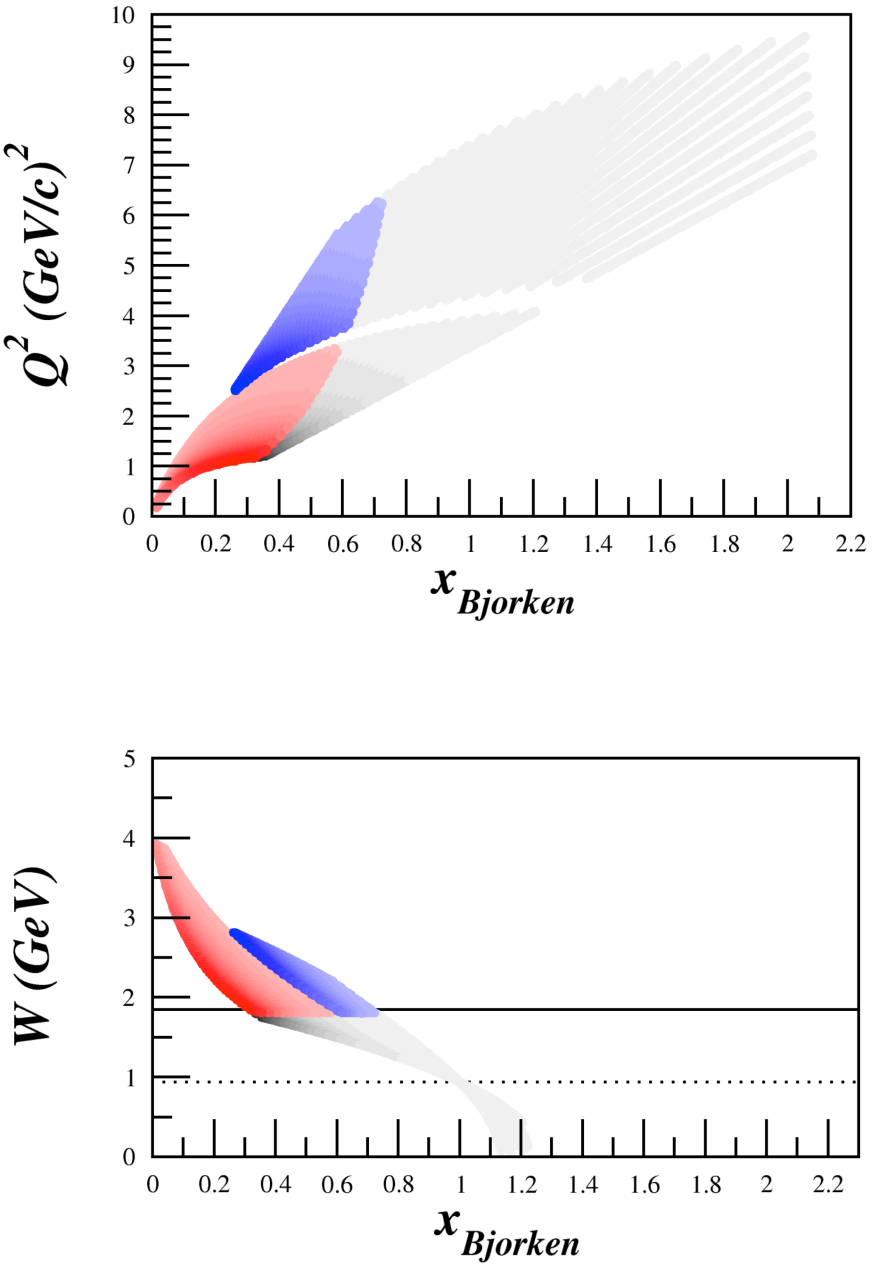

Figure 10: Kinematic coverage for incident beam energy of 8.8 GeV. The red points are for the forward detector and the blue are for the backward detector. The black/grey settings are not included in our rates estimates since they fall below $W \geq$1.85GeV.

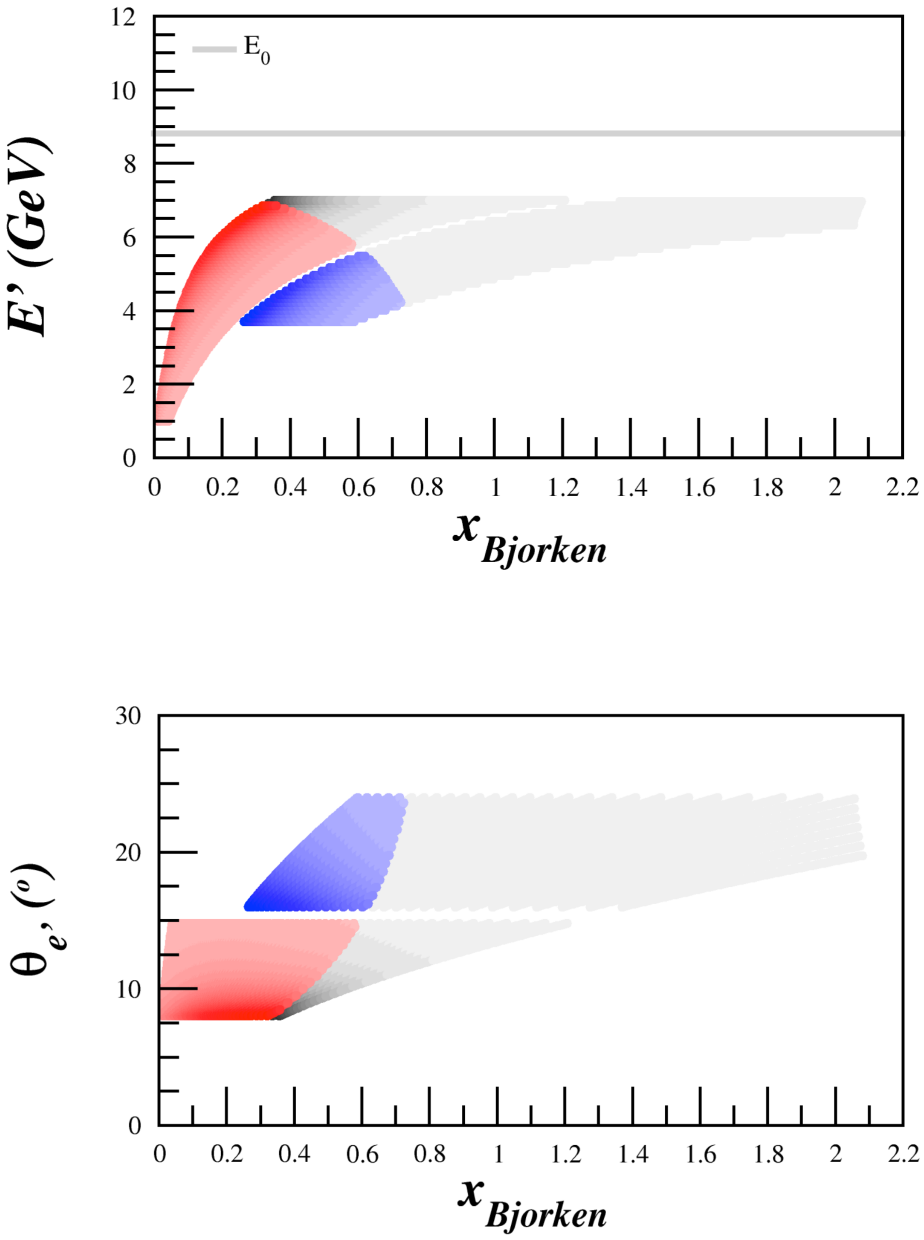

Figure 11: Kinematic coverage for incident beam energy of 8.8 GeV. The red points are for the forward detector and the blue are for the backward detector. The black/grey settings are not included in our rates estimates since they fall below $W \geq$1.85GeV.

2.1 Experimental Method

The measured DIS double differential cross section for a spin-1 target characterized by a vector polarization P_z and tensor polarization P_{zz} is expressed as,

$$\frac{d^2\sigma_p}{dxdQ^2} = \frac{d^2\sigma}{dxdQ^2}\left(1 - P_z P_B A_1 + \frac{1}{2}P_{zz}A_{zz}\right), \tag{12}$$

where, σ_p (σ) is the polarized (unpolarized) cross section, P_B is the incident electron beam polarization, and A_1 (A_{zz}) is the vector (tensor) asymmetry of the virtual-photon deuteron cross section. This allows us to write the positive polarized tensor, $0 < P_{zz} \leq 1$, asymmetry using unpolarized electron beam as,

$$A_{zz} = \frac{2}{P_{zz}}\left(\frac{\sigma_1}{\sigma} - 1\right) \tag{13}$$

where σ_1 is the polarized cross section for

$$P_{zz} = \frac{n_+ - 2n_0 + n_-}{n_+ + n_- + n_0}, \text{ for } n_+ + n_- > 2n_0. \tag{14}$$

Here n_m represents the portion of the ensemble in the m state.

Eq. 13 reveals that the asymmetry A_{zz} compares two different cross sections measured under different polarization conditions of the target, positively tensor polarized and unpolarized. To obtain the relative cross section measurement in the same configuration, the same target cup and material will be used at alternating polarization states (polarized vs. unpolarized), and the magnetic field providing the quantization axis will be oriented along the beamline at all times. This field will always be held at the same value, regardless of the target material polarization state. This ensures that the acceptance remains consistent within the stability (10^{-4}) of the super conducting magnet.

Since many of the factors involved in the cross sections cancel in the ratio, Eq. 13 can be expressed in terms of the charge normalized, efficiency corrected numbers of tensor polarized N_1^c and unpolarized N^c counts,

$$A_{zz} = \frac{2}{fP_{zz}}\left(\frac{N_1^c}{N^c} - 1\right) \tag{15}$$

The dilution factor f corrects for the presence of unpolarized nuclei in the target.

The measured tensor asymmetry allows for an extraction of the tensor structure function b_1 using the world data on the leading-twist structure function F_1^d,

$$b_1 = -\frac{3}{2}F_1^d A_{zz} \tag{16}$$

In Eq. 15, the dilution factor is defined as,

$$f = \frac{N_D\sigma_D}{N_N\sigma_N + N_D\sigma_D + \Sigma N_A\sigma_A}, \tag{17}$$

where N_D is the number of deuterium nuclei in the target and σ_D is the corresponding inclusive double differential scattering cross section, N_N is the nitrogen number of scattered nuclei with

Source	Systematic
Polarimetry	8.0%
Dilution/packing fraction	4.0%
Radiative corrections	1.5%
Charge Determination	1.0%
Detector resolution and efficiency	1.0%
Total	9.2%

Table 4: Estimates of the scale dependent contributions to the systematic error of A_{zz}.

cross section σ_N, and N_A is the numbers of other scattering nuclei of mass number A with cross section σ_A. The denominator of the dilution factor can be written in terms of the relative volume ratio of ND_3 to LHe in the target cell, otherwise known as the packing fraction p_f. In our case of a cylindrical target cell oriented along the magnetic field, the packing fraction is exactly equivalent to the percentage of the cell length filled with ND_3. The dilution factor is discussed in further detail in Sec. 2.2.3.

The time necessary to achieve the desired precision δA is:

$$T = \frac{N_T}{R_T} = \frac{16}{P_{zz}^2 f^2 \delta A_{zz}^2 R_T} \tag{18}$$

where R_T is the total rate and $N_T = N^1 + N$ is the total estimated number of counts to achieve the uncertainty δA_{zz}.

2.1.1 Statistical Uncertainty

To investigate the statistical uncertainty we start with the equation for A_{zz} using measured counts for polarized data N_1 and unpolarized data N,

$$A_{zz} = \frac{2}{f P_{zz}} \left(\frac{N_1}{N} - 1 \right). \tag{19}$$

The absolute error with respect to counts in then,

$$\delta A_{zz} = \frac{2}{f P_{zz}} \sqrt{\left(\frac{\delta N_1}{N} \right)^2 + \left(\frac{N_1 \delta N}{N^2} \right)^2}. \tag{20}$$

For small asymmetries, $N_1 \approx N$, so that twice N is required to obtain the total number of counts N_T for the experiment. This leads to:

$$\delta A_{zz} = \frac{4}{f P_{zz}} \frac{1}{\sqrt{N_T}}. \tag{21}$$

2.1.2 Systematic Uncertainty

Table 4 shows a list of the scale dependent uncertainties contributing to the systematic error in A_{zz}. With careful minimization, the uncertainty in P_z can be held to better than 4%, as demonstrated in the g2p/GEp experiment [23]. This leads to a relative uncertainty in P_{zz} of 7.7%. Alternatively, the tensor asymmetry can be directly extracted from the NMR lineshape as discussed in Sec. 2.2, with similar uncertainty. The uncertainty from the dilution factor and packing fraction of the ammonia target contributes at the 4% level. The systematic effect on A_{zz} due to the QED radiative corrections will be quite small. For our measurement there will be no polarized radiative corrections at the lepton vertex, and the unpolarized corrections are known to better than 1.5%. Charge calibration and detector efficiencies are expected to be known better to 1%, but the impact of time-dependent drifts in these quantities must be carefully controlled.

Time dependent factors

Eq. 15 involves the ratio of counts, which leads to cancellation of several first order systematic effects. However, the fact that the two data sets will not be taken simultaneously leads to a sensitivity to time dependent variations which will need to be carefully monitored and suppressed. To investigate the systematic differences in the time dependent components of the integrated counts, we need to consider the effects from calibration, efficiency, acceptance, and luminosity between the two polarization states.

In order to look at the effect on A_{zz} due to drifts in beam current measurement calibration and detector efficiency, we rewrite Eq. 15 explicitly in terms of the raw measured counts N_1 and N,

$$\begin{aligned} A_{zz} &= \frac{2}{fP_{zz}}\left(\frac{N_1^c}{N^c}-1\right) \\ &= \frac{2}{fP_{zz}}\left(\frac{Q\varepsilon l\mathcal{A}}{Q_1\varepsilon_1 l\mathcal{A}}\frac{N^1}{N}-1\right) \end{aligned} \tag{22}$$

where Q represents the accumulated charge, and ε is the detector efficiency. The target length l and acceptance $\mathcal{A}$ are identical in both states, to first order.

We can then express Q_1 as the change in beam current measurement calibration that occurs in the time it takes to collect data in one polarization state before switching such that $Q_1 = Q(1-\delta Q)$. In this notation, δQ is a dimensionless ratio of charges in the different polarization states. A similar representation is used for drifts in detector efficiency leading to,

$$A_{zz} = \frac{2}{fP_{zz}}\left(\frac{N_1 Q(1-\delta Q)\varepsilon(1-\delta\varepsilon)}{NQ\varepsilon}-1\right). \tag{23}$$

which leads to,

$$A_{zz} = \frac{2}{fP_{zz}}\left(\frac{N_1}{N}(1-\delta Q-\delta\varepsilon+\delta Q\delta\varepsilon)-1\right). \tag{24}$$

We can obtain estimates of δQ and $\delta\varepsilon$ from previous experiments. For the HRS detector drift during the JLab transversity experiment E06-010, the detector response was measured such that the normalized yield for the same condition over a three month period indicated little change ($< 1\%$). These measurements indicated that for the short time (20 minutes) between target spin flips, the

detector drift should be less than 1% times the ratio of the time period between target spin flips and three months.

For the present proposal, we use the same estimate except that the period between target polarization states is ≈12 hours leading to an overall drift $\delta\varepsilon \sim 0.01\%$. A similar approach can be used to establish an estimate for δQ using studies from the data from the (g2p/GEp) experiment, resulting in $\delta Q \sim 0.01\%$.

To express A_{zz} in terms of the estimated experimental drifts in efficiency and current measurement we can write,

$$A_{zz} = \frac{2}{fP_{zz}}\left(\frac{N_1}{N} - 1\right) \pm \frac{2}{fP_{zz}}\delta\xi. \tag{25}$$

where $\delta\xi = \delta Q + \delta\varepsilon$. This leads to a contribution to A_{zz} on the order of 1×10^{-3},

$$dA_{zz}^{drift} = \pm\frac{2}{fP_{zz}}\delta\xi = \pm 3.7 \times 10^{-3}. \tag{26}$$

The polarization state of the target will be changed every 12 hours, so each of our settings will involve between $N = 12$ to $N = 60$ polarization cycle pairs. This further suppreses the effect of any drift to less than the 10^{-3} level. Though a very important contribution to the error, this value allows a clean measurement of $A_{zz} = 0$ at $x = 0.45$ without overlap with the Hermes error bar. For this estimate we assumed only two polarization state changes in a day. Increasing this rate decreases the systematic effect in A_{zz} accordingly, but at the cost of increased overhead.

Detector efficiencies can drift for a variety of reasons, including fluctuations in gas quality, high voltage drift, or drifts in the spectrometer magnetic fields. All of these types of variation can be controlled and minimized during the experiment through careful monitoring as well as systematic studies of the data collected.

The identical configuration of the two polarization states minimizes the relative changes in luminosity with respect to time. Consistency checks on the measured cross section data can be implemented to ensure the quality of each run used in the asymmetry analysis. Fluctuations in luminosity due to target density variation can be kept to a minimum by keeping the material beads at the same temperature for both polarization states through control of the microwave and the LHe evaporation. The He vapor pressure reading provides an accuracy of material temperature changes at the level of ∼0.1%. Beam rastering can also be controlled to a high degree.

The dominant source of any variation in acceptance $\mathcal{A}$ from state to state will be the stability of the target magnetic field. The capacity to set and hold the target super conducting magnet to a desired holding field is $\delta B/B$ =0.01%. The same target cup will be used for each state, which removes any variation in the target length l.

2.1.3 Overhead

Table 5 summarizes the expected overhead, which sums to 3.0 days. The dominant overhead comes from switching from the polarized to unpolarized state and vice versa. Target anneals will need to be performed about every other day, and the material replaced once a week. Measurements of the dilution from the unpolarized materials contained in the target, and of the packing fraction due to the granular composition of the target material will be performed with a carbon target.

Overhead	Number	Time Per (hr)	(hr)
Polarization/depolarization	8	2.0	16.0
Target anneal	4	4.0	16.0
Target T.E. measurement	4	4.0	16.0
Target material change	2	1.0	2.0
Packing Fraction/Dilution runs	4	1.0	4.0
BCM calibration	2	2.0	4.0
Optics	2	4.0	8.0
Linac change	1	8.0	8.0
			3.0 days

Table 5: Contributions to the experimental overhead.

2.2 Polarized Target

This experiment will use the JLab/UVa dynamically polarized solid ND_3 target operated in longitudinal mode. The target is typically operated with a specialized slow raster, and beamline instrumentation capable of characterizing the low current 50-115 nA beam. All of these requirements have been met previously in Hall A for the E08-027/E08-007 run.

The target operates on the principle of Dynamic Nuclear Polarization, to enhance the low temperature (1 K), high magnetic field (5 T) polarization of solid materials by microwave pumping. The polarized target assembly contains several target cells of 3.0 cm length that can be selected individually by remote control to be located in the uniform field region of a superconducting Helmholtz pair. The permeable target cells are immersed in a vessel filled with liquid Helium and maintained at 1 K by use of a high power evaporation refrigerator.

The target material is exposed to microwaves to drive the hyperfine transition which aligns the nucleon spins. The heating of the target by the beam causes a drop of a few percent in the polarization, and the polarization slowly decreases with time due to radiation damage. Most of the radiation damage can be repaired by periodically annealing the target, until the accumulated dose reached is greater than about 0.5×10^{17} e^-/cm^2, at which time the target material needs to be replaced.

2.2.1 Polarization Analysis

The three Zeeman sublevels of the deuteron system ($m = -1, 0, 1$) are shifted unevenly due to the quadrupole interaction [3]. This shift depends on the angle between the magnetic field and the electrical field gradient, and gives rise to two separate transition energies. Hence, the unique double peaked response displayed in Fig. 13.

The energies [24] of these three magnetic sublevels are:

$$E = -h\nu_D m + h\nu_Q \left[(3\cos^2(\theta) - 1\right] \left[3m^2 - I(I+1)\right] \tag{27}$$

where ν_D is the deuteron Larmor frequency and ν_Q is a function of the deuteron quadrupole moment eQ. The quadrupole interaction shifts these levels depending on the angle θ between the magnetic field and the electrical field gradient, as shown in Fig. 14.

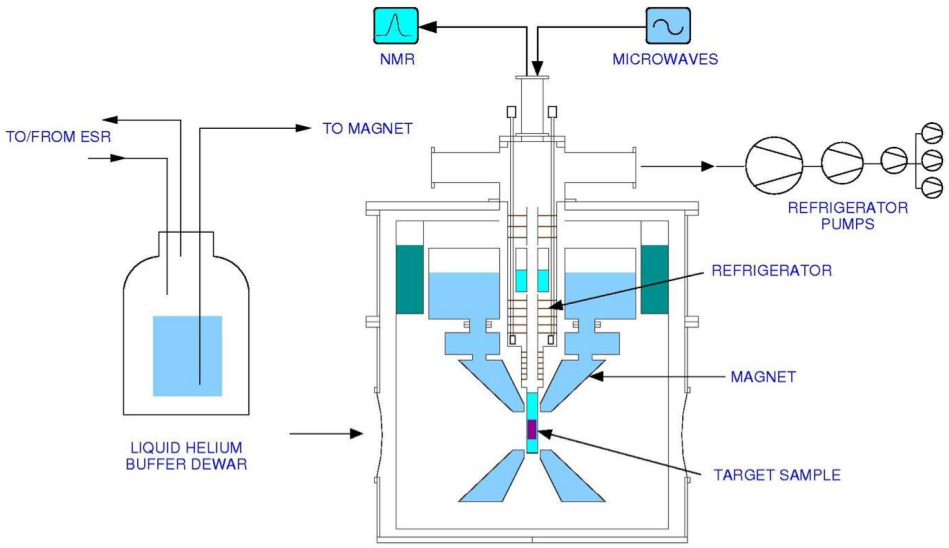

Figure 12: Cross section view of the JLab/UVa polarized target. Figure courtesy of C. Keith.

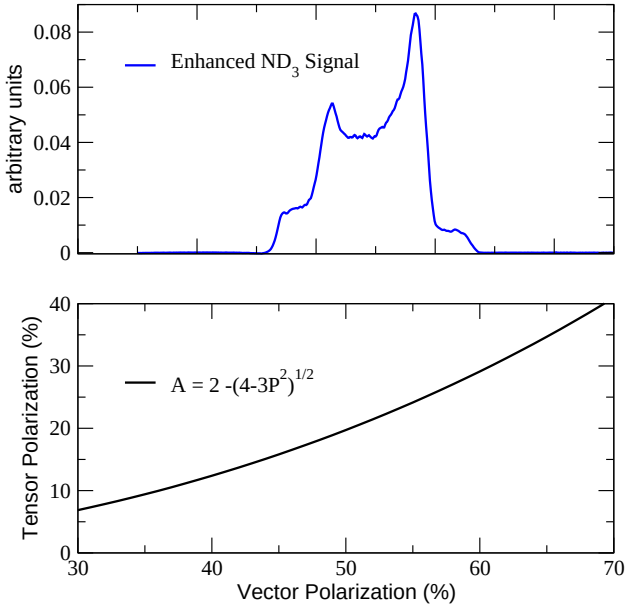

Figure 13: **Top**: NMR signal for ND_3 with a vector polarization of approximately 50% from the GEN experiment. **Bottom**: Relationship between vector and tensor polarization in equilibrium, and neglecting the small quadrupole interaction.

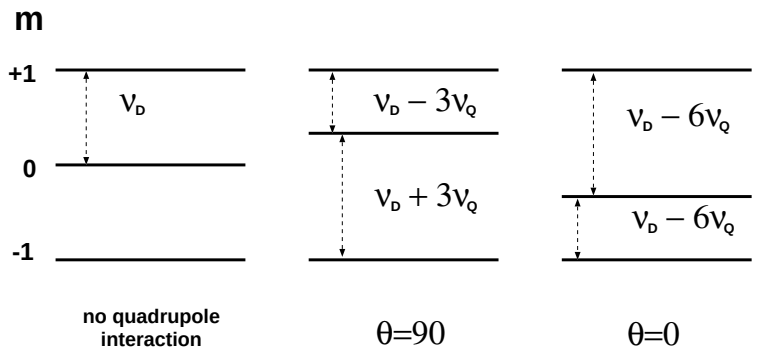

Figure 14: Energy levels in ND_3. The level spacing is shifted by the quadrupole interaction, which depends on the angle θ between the magnetic field and the electric field gradient.

When the system is at thermal equilibrium with the solid lattice, the deuteron polarization is known from:

$$P_z = \frac{4 + \tanh \frac{\mu B}{2kT}}{3 + \tanh^2 \frac{\mu B}{2kT}} \tag{28}$$

where μ is the magnetic moment, and k is Boltzmann's constant. The vector polarization can be determined by comparing the enhanced signal with that of the TE signal (which has known polarization). This polarimetry method is typically reliable to about 5% relative.

Similarly, the tensor polarization is given by:

$$P_{zz} = \frac{4 + \tanh^2 \frac{\mu B}{2kT}}{3 + \tanh^2 \frac{\mu B}{2kT}} \tag{29}$$

From Eqs. 28 and 29, we find:

$$P_{zz} = 2 - \sqrt{4 - 3P_z^2}$$

In addition to the TE method, polarizations can be determined by analyzing NMR lineshapes as described in [25] with a typical 7% relative uncertainty. At high polarizations, the intensities of the two transitions differ, and the NMR signal shows an asymmetry R in the value of the two peaks, as shown in Fig. 13. The vector polarization is then given by:

$$P_z = \frac{R^2 - 1}{R^2 + R + 1} \tag{30}$$

and the tensor polarization is given by:

$$P_{zz} = \frac{R^2 - 2R + 1}{R^2 + R + 1} \tag{31}$$

The DNP technique produces deuteron vector polarizations of up to 60% in ND_3 and 64% in LiD [26], which corresponds to tensor polarizations of approximately 30%. The target polarization decays while in beam, so that the average polarization is less than this.

2.2.2 Depolarizing the Target

To move from polarized to unpolarized measurements, the target polarization will be annihilated using destructive NMR loop field changes and destructive DNP microwave pumping. It is also possible to remove LHe in the nose of the target to remove the polarization by heating. During unpolarized data taking the incident electron beam heating is enough to remove the thermal equilibrium polarization.

NMR measurements will be used to confirm destruction of the polarization. The target material will be held at a constant temperature, and the target field will be held at a constant magnitude for both polarized and unpolarized data collection. in order to minimize the systematic differences in the two states. To minimize systematic effects over time, the polarization condition will be switched twice in a 24 hour period.

2.2.3 The Dilution Factor

To derive the expression for the dilution factor, we first start with the ratio of polarized to unpolarized counts. In each case, the number of counts that are actually measured, neglecting the small contributions of the thin aluminium cup window materials, NMR coils, etc., are

$$N_1 = Q_1 \varepsilon_1 \mathcal{A}_1 l_1 [(\sigma_N + 3\sigma_1) p_f + \sigma_{He}(1 - p_f)], \tag{32}$$

and

$$N = Q \varepsilon \mathcal{A} l [(\sigma_N + 3\sigma) p_f + \sigma_{He}(1 - p_f)]. \tag{33}$$

where Q represents accumulated charge, ε is the dectector efficiency, $\mathcal{A}$ the cup acceptance, and l the cup length.

For this calculation we assume similar charge accumulation such that $Q \simeq Q_1$, and that the efficiencies stay constant, in which case all factors drop out of the ratio leading to

$$\begin{aligned}
\frac{N_1}{N} &= \frac{(\sigma_N + 3\sigma_1) p_f + \sigma_{He}(1 - p_f)}{(\sigma_N + 3\sigma) p_f + \sigma_{He}(1 - p_f)} \\
&= \frac{(\sigma_N + 3\sigma(1 + A_{zz} P_{zz}/2)) p_f + \sigma_{He}(1 - p_f)}{(\sigma_N + 3\sigma) p_f + \sigma_{He}(1 - p_f)} \\
&= \frac{[(\sigma_N + 3\sigma) p_f + \sigma_{He}(1 - p_f)] + 3\sigma p_f A_{zz} P_{zz}/2}{(\sigma_N + 3\sigma) p_f + \sigma_{He}(1 - p_f)} \\
&= 1 + \frac{3\sigma p_f A_{zz} P_{zz}/2}{(\sigma_N + 3\sigma) p_f + \sigma_{He}(1 - p_f)} \\
&= 1 + \frac{1}{2} f A_{zz} P_{zz},
\end{aligned} \tag{34}$$

where $\sigma_1 = \sigma(1 + A_{zz} P_{zz}/2)$ has ben substituted, per Eq. 12, with $P_B = 0$. It can be seen that the above result corresponds to Eq. 15.

2.2.4 Prospects for Improving the Tensor Polarization

We've assumed a tensor polarization of 25% in this proposal. This is just the tensor polarization that occurs in a standard P_z= 56% vector polarized ND_3 target according to Eq. 30. This enables a

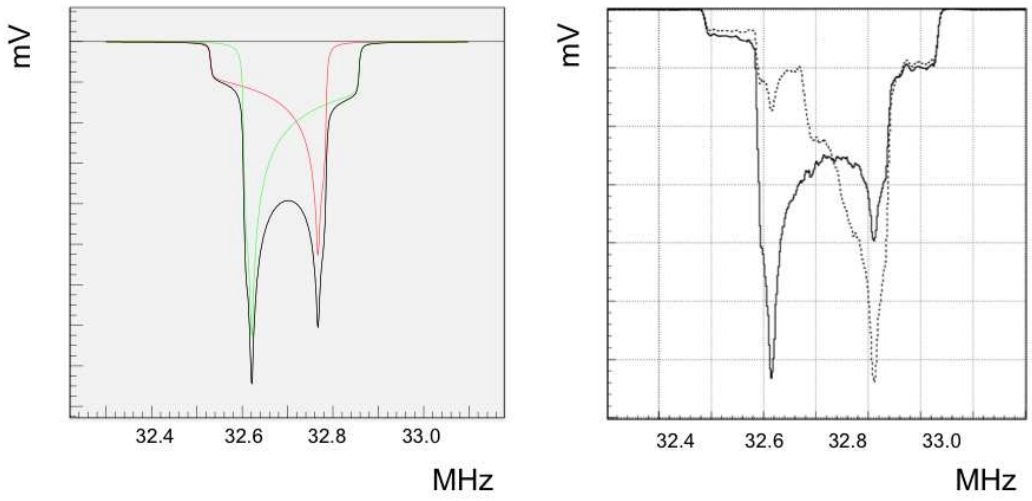

Figure 15: **Left**: Model prediction [25] of the NMR response for an ND_3 sample. The two discrete transitions (red and green) blend into the characteristic double peaked structure. **Right** : Demonstration of RF hole burning in ND_3. Solid line: ND_3 sample with about 30% vector polarization. Dashed line: the same sample after application of a saturating RF field, which raised the tensor polarization to $P_{zz} \approx 30\%$. Notice the strong suppression of the left peak. Reproduced from [27].

significant measurement of $b_1(x)$, as shown in Fig. 6 and Fig. 7. Any improvement to the expected polarization, although not strictly necessary, would allow the addition of kinematic points, and/or improved statistical accuracy.

With this in mind, we note that there is a concerted effort at the University of New Hampshire and the University of Virginia to directly enhance tensor polarization by disturbing the thermal equilibrium of the sample using a frequency modulated RF source to stimulate transitions from the m=0 level. This technique is known as semi-selective RF saturation. This changes the population of the m=0 level, thus changing the tensor asymmetry. This method of 'hole burning' the NMR line with a saturating RF field was demonstrated by deBoer [28], and Meyer [24, 3] in 1985, with more recent successes demonstrated at both UNH and UVa.

In light of this, we are optimistic that we will eventually be capable of producing tensor polarizations of 35% and higher, although we have not assumed it in this Letter of Intent.

3 Summary

We request 14 days of production beam at 6.6 GeV and 8.8 GeV, in order to measure the tensor asymmetry A_{zz} and the spin structure function b_1 using a tensor polarized (P_{zz}=25%) deuteron target together with the Hall A SoLID detector. Half of the total PAC days will be spent at each incident energy. The 6.6 GeV data will be taken simultaneously with a quasi-elastic measurement of Azz, which is being submitted as a separate Letter of Intent (LOI). The UVa solid polarized ND_3 target will be used, along with the Hall A SoLID detector, and an unpolarized 100 nA beam. An additional 3.0 days will be needed for overhead. We are submitting this as an LOI because we have

not yet run a full simulation of the SoLID detector. Instead we have approximated rates based on the average acceptance and detector characteristics. Weve assumed a tensor polarization of 25% in this proposal, although there is an active program to increase this number significantly.

We can determine b_1 with sufficient precision to discriminate between conventional nuclear models, and the more exotic behavior which is hinted at by the HERMES data. This experiment will provide access to the tensor quark polarization and allow a test of the Close-Kumano sum rule, which vanishes in the absence of tensor polarization in the quark sea. Until now, tensor structure has been largely unexplored, so the study of these quantities holds the potential of initiating a new field of spin physics at Jefferson Lab.

References

[1] H. Khan and P. Hoodbhoy, Phys. Rev. **C44**, 1219 (1991).

[2] S. K. Taneja, K. Kathuria, S. Liuti, and G. R. Goldstein, Phys.Rev. **D86**, 036008 (2012).

[3] W. Meyer *et al.*, Nucl. Instrum. Meth. **A244**, 574 (1986).

[4] J. Carlson and R. Schiavilla, Rev. Mod. Phys. **70**, 743 (1998).

[5] J. L. Forest *et al.*, Phys. Rev. **C54**, 646 (1996).

[6] A. Pais, Phys. Rev. Lett. **19**, 544 (1967).

[7] L. L. Frankfurt and M. I. Strikman, Nucl. Phys. **A405**, 557 (1983).

[8] P. Hoodbhoy, R. L. Jaffe, and A. Manohar, Nucl. Phys. **B312**, 571 (1989).

[9] C. Riedl, Ph. D thesis, DESY-THESIS-2005-027 (2005).

[10] A. Airapetian *et al.*, Phys. Rev. Lett. **95**, 242001 (2005).

[11] J. Edelmann, G. Piller, and W. Weise, Phys. Rev. **C57**, 3392 (1998).

[12] K. Bora and R. L. Jaffe, Phys. Rev. **D57**, 6906 (1998).

[13] S. Kumano, Phys. Rev. **D82**, 017501 (2010).

[14] G. A. Miller, In Stanford 1989, Proceedings, Electronuclear physics with internal targets 30-33 .

[15] G. A. Miller, private communication, to be published.

[16] P. J. Sutton, A. D. Martin, R. G. Roberts, and W. J. Stirling, Phys. Rev. **D45**, 2349 (1992).

[17] A. Y. Umnikov, Phys. Lett. **B391**, 177 (1997).

[18] M. Sargsian, private communication, to be published.

[19] L. L. Frankfurt and M. I. Strikman, Phys. Rept. **76**, 215 (1981).

[20] M. M. Sargsian, S. Simula, and M. I. Strikman, Phys. Rev. **C66**, 024001 (2002).

[21] F. E. Close and S. Kumano, Phys. Rev. **D42**, 2377 (1990).

[22] A. V. Efremov and O. V. Teryaev, Sov. J. Nucl. Phys. **36**, 557 (1982).

[23] D. Keller, "Uncertainty in DNP Target Data for E08-007", JLab-TN-051.

[24] W. Meyer and E. Schilling, BONN-HE-85-06, C84-09-03.1 (1985).

[25] C. Dulya *et al.*, Nucl. Instrum. Meth. **A398**, 109 (1997).

[26] S. L. Bueltmann *et al.*, Nucl. Instrum. Meth. **A425**, 23 (1999).

[27] S. Bueltmann, D. Crabb, Y. Prok. *UVa Target Studies*, UVa Polarized Target Lab technical note, 1999.

[28] W. de Boer, Cern Report CERN-74-11 (1974).